PHYSICAL REVIEW B **73**, 085415 (2006)

Static and dynamic Jahn-Teller effect in the alkali metal fulleride salts A_4C_{60} (A=K,Rb,Cs)

G. Klupp* and K. Kamarás†
Research Institute for Solid State Physics and Optics, Hungarian Academy of Sciences, P.O. Box 49, H-1525 Budapest, Hungary

N. M. Nemes‡ and C. M. Brown
NIST Center for Neutron Research, Gaithersburg, Maryland 20899-8562, USA
and Department of Materials Science and Engineering, University of Maryland, College Park, Maryland 20742, USA

J. Leão
NIST Center for Neutron Research, Gaithersburg, Maryland 20899-8562, USA
(Received 24 October 2005; revised manuscript received 6 January 2006; published 16 February 2006)

We report the temperature dependent mid- and near-infrared spectra of K_4C_{60}, Rb_4C_{60}, and Cs_4C_{60}. The splitting of the vibrational and electronic transitions indicates a molecular symmetry change of C_{60}^{4-} which brings the fulleride anion from D_{2h} to either a D_{3d} or a D_{5d} distortion. In contrast to Cs_4C_{60}, low temperature neutron diffraction measurements did not reveal a structural phase transition in either K_4C_{60} and Rb_4C_{60}. This proves that the molecular transition is driven by the molecular Jahn-Teller effect, which overrides the distorting potential field of the surrounding cations at high temperature. In K_4C_{60} and Rb_4C_{60} we suggest a transition from a static to a dynamic Jahn-Teller state without changing the average structure. We studied the librations of these two fullerides by temperature dependent inelastic neutron scattering and conclude that both pseudorotation and jump reorientation are present in the dynamic Jahn-Teller state.

DOI: 10.1103/PhysRevB.73.085415 PACS number(s): 61.48.+c, 71.70.Ch, 71.70.Ej, 78.30.Na

I. INTRODUCTION

The insulating character of the A_4C_{60} (A=K,Rb,Cs) compounds has been a longstanding puzzle in fullerene science. The successful description involves a combination of the molecular Jahn-Teller (JT) effect and the Mott-Hubbard band picture resulting in the theory of the nonmagnetic Mott-Jahn-Teller insulating state.[1] This theory has been used effectively for the explanation of electron energy-loss spectroscopy (EELS)[2,3] and NMR[4] measurements on A_4C_{60}. Recently, a highly refined experiment[5] by scanning tunneling microscopy has revealed JT distorted molecules in K_4C_{60} monolayers. In macroscopic crystals, however, the distortion could only be detected directly in one case: anions with D_{2h} symmetry were found in Cs_4C_{60} by neutron diffraction.[6] In Cs_4C_{60}, x-ray[7] and neutron diffraction measurements also found an orthorhombic-tetragonal (*Immm* to *I*4/*mmm*) phase transition between 300 and 623 K. The crystal structure of K_4C_{60} and Rb_4C_{60} was determined to be *I*4/*mmm* at room temperature,[8,9] although atomic positions were not refined. In the case of K_4C_{60} midinfrared (MIR) and near-infrared (NIR) measurements showed a splitting that indicated a JT distorted anion.[10] The distortion was found to be temperature dependent[11] and the possibility of a similar phase transition as that in Cs_4C_{60} has been put forward.

Vibrational spectroscopy is uniquely sensitive to the change in molecular symmetry (i.e., the exact shape of the molecule) through the splitting of vibrational bands. Because it detects the motion of atoms, it naturally goes beyond the spherical approximation used for crude models of the electronic structure. In this respect, molecular vibrations are more intimately connected to structural studies which show the average position of the atomic cores than to methods probing magnetic and electronic excitations where an analogy to atomic orbitals is often sufficient to describe the results. In this paper, we follow the distortions of fulleride ions in three A_4C_{60} salts (A=K,Rb,Cs) with temperature. Our conclusions are mainly drawn from midinfrared vibrational spectra, but we also study the effect of these distortions on electronic orbitals of the C_{60}^{4-} ions, through NIR spectra probing both intra- and intermolecular electronic excitations. To clarify whether the distortions are caused by crystal potential or molecular degrees of freedom, we performed temperature-dependent neutron diffraction studies, complemented by inelastic neutron scattering in order to detect molecular motion. We find no structural phase transition to a cooperative static Jahn-Teller state in either K_4C_{60} or Rb_4C_{60} down to 4 K; changes in vibrational spectra reflect the change in molecular symmetry and thus a transition from static to dynamic Jahn-Teller state as the temperature is raised.

II. THE JAHN-TELLER EFFECT IN FULLERIDE SALTS

To understand the precise nature of the distortions occurring in fulleride salts, we have to elaborate on the details of their crystal and molecular symmetry. An entire monograph has been devoted to this question,[12] here we will only repeat the main statements.

The Jahn-Teller effect is caused by the interaction of a degenerate electronic state with molecular vibrations.[13] In C_{60} anions, the electronic states involved are those of the triply degenerate t_{1u} orbitals and the vibrations are the ten fivefold degenerate H_g modes. These interactions result in a change of shape of the molecule and consequently a change in the splitting of the electronic orbitals. Electrons will occupy the lowest-energy levels and thus, if the splitting is large enough, overcome Hund's rule and form nonmagnetic systems.

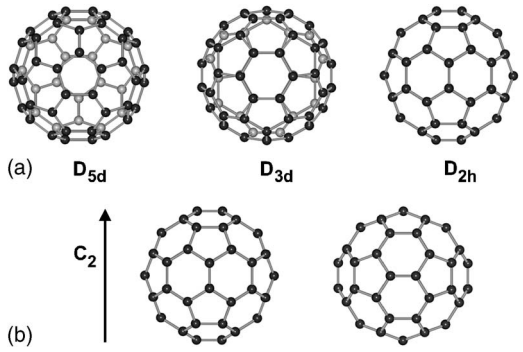

FIG. 1. (a) Possible Jahn-Teller distortions in fulleride ions. The axis along which the distortion occurs is perpendicular to the plane of the paper through the center of the molecule. The atoms above the plane of the paper are black while those under it are gray. (b) The two standard orientations in fullerene/fulleride solids. The z crystal axis coincides with the C_2 molecular axis shown.

In most solids containing open-shell species, the energy bands are much broader than the JT splitting; this is why the A_3C_{60} salts are metals.[14] In this case the electrons cannot be assigned to individual molecules and therefore Jahn-Teller coupling is not possible. The insulating character of A_4C_{60} salts has been proposed to be caused by Mott localization which enables Jahn-Teller coupling between the localized electrons and the vibrational degrees of freedom. This state has been termed the "Mott-Jahn-Teller nonmagnetic insulator."[1] As we will see, our results fully support this picture, so we describe the A_4C_{60} systems in this framework.

In the atomic orbital-like classification used by Chancey and O'Brien,[12] the C_{60}^{4-} molecular ion is a $p^4 \otimes h$ system, where the allowed Jahn-Teller distortions for isolated ions are D_{2h}, D_{3d}, and D_{5d}. The predicted shape of the distortions is "pancake-type:" a flattening along a C_2, C_3, or C_5 molecular axis.[12] We illustrate these possible distortions in Fig. 1(a). The adiabatic potential energy surface (APES) of these systems has minima at either D_{3d} or D_{5d} symmetry, and saddle points at D_{2h} symmetry.[15] If the D_{3d} geometries are minima, then the D_{5d} are maxima and vice versa. There are six possible D_{5d} distortions and ten D_{3d} distortions in different directions; transitions between them occur through tunneling which results in a different molecular shape without the rotation of the molecule itself.[16] This motion is called *pseudorotation*. Proof of such dynamic distortions has indeed been presented recently by a sophisticated experiment on monoanions produced in a storage ring.[17] The D_{2h} distortion can only be realized when an external potential lowers the energy of this distortion. Forming a solid from fulleride ions with counterions creates such a potential field.

Apart from the intrinsic JT distortion, forcing an icosahedral C_{60} molecule into a crystal inevitably lowers its symmetry. For all crystal systems with orthogonal principal axes and one molecule per primitive unit cell the C_2 symmetry axes of the molecule are aligned with the crystallographic axes, but the molecule can assume two different orientations as shown in Fig. 1(b). These are the standard orientations originally defined for orientationally ordered C_{60}.[18] Thus for a C_{60}^{n-} anion the x and y molecular axes are not equivalent, reflecting the lack of a fourfold axis in icosahedral symmetry.

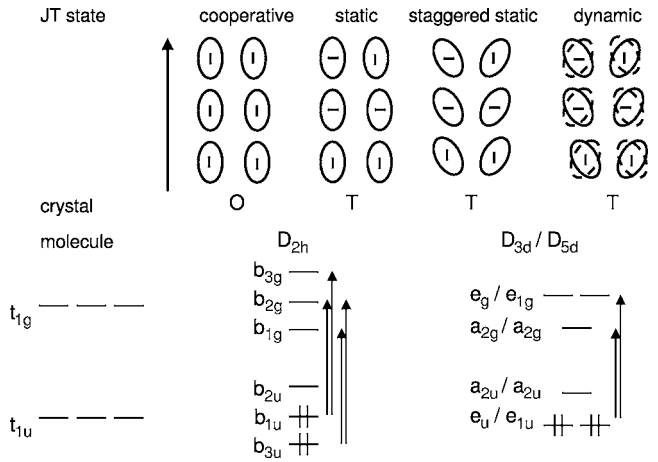

FIG. 2. Top: Some possible arrangements of fulleride ions in the crystal structures in A_4C_{60} systems and their molecular distortions. Ellipses with horizontal and vertical bars, respectively, represent the standard orientations in Fig. 1(b). O stands for orthorthombic, T for tetragonal crystal structure. Bottom: splitting of the HOMO (t_{1u}) and the LUMO (t_{1g}) molecular orbitals of C_{60}^{4-} in a D_{2h} (cooperative static, static) and D_{3d} or D_{5d} (staggered static, dynamic) distorted molecule, respectively. Infrared-active vibrations of T_{1u} symmetry show similar splitting. Arrows denote dipole allowed transitions between split states.

Nevertheless, the misconception prevailed in the early fullerene literature that in a tetragonal distorting field, the *individual molecular ions* can be uniaxially distorted into the D_{4h} pointgroup with the c crystal axis as the principal axis.[19–21] This approach treats the fulleride ions as a sphere[22] (a "giant atom"), and takes the effect of the distorting crystal field to be the same as the inherent JT distortion of the balls, leading to the conclusion that the two are indistinguishable. It is apparent from structural studies, however,[8,9] that in a tetragonal system the C_{60} molecules cannot be equivalent. Orbital overlap between cations and anions determines whether the balls are ordered or disordered, i.e., the crystal is tetragonal or orthorhombic,[6,23,24] but the molecular symmetry is the same D_{2h} in both cases. The consequence is that the threefold degenerate orbitals will show a threefold splitting in both an orthorhombic and tetragonal environment. An orthorhombic crystal is formed by simply arranging the D_{2h} distorted molecules in an ordered fashion, while the overall tetragonal symmetry of the crystal can only be maintained as an average with some sort of disorder, either static or dynamic.[9] In the following we try to summarize the possible arrangements and relate them to the crystal structures as classified by Fabrizio and Tosatti.[1] Note that we consciously avoid the use of the term *merohedral disorder* throughout the discussion: this concept is correctly used for A_3C_{60} systems[25] but is incorrect for A_4C_{60}.

The ordered orthorhombic structure mentioned above is the so-called *cooperative static Jahn-Teller state*. For the overall symmetry to become tetragonal, we have to assume there exists an average (spatial or temporal) of several molecules. We summarize the situation in Fig. 2. The static disorder means that all molecules align their C_2 axes in the c direction, but the hexagon-hexagon bonds are randomly ori-

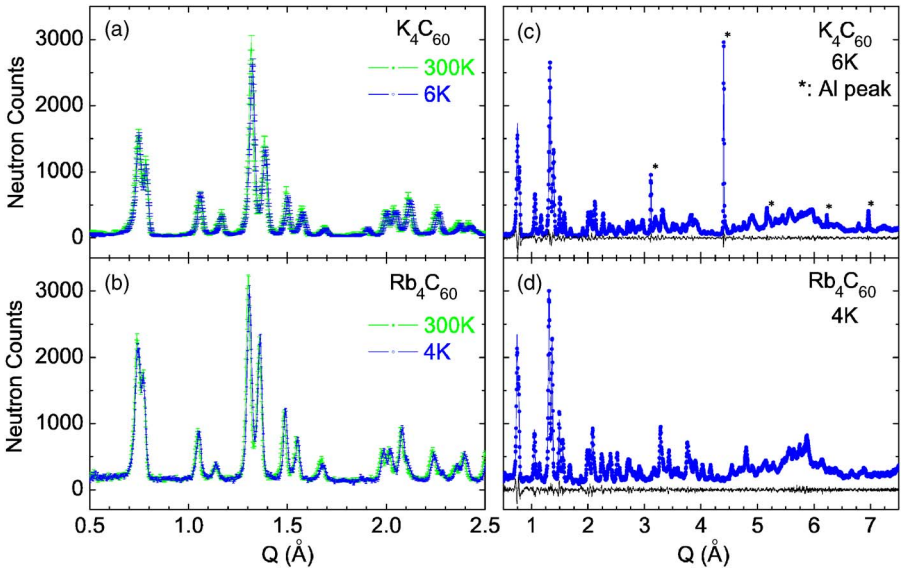

FIG. 3. (Color online) Neutron diffraction profiles of (a) K_4C_{60} and (b) Rb_4C_{60} at two temperatures, showing only a small thermal contraction of the lattice but no change in symmetry or unit cell. LeBail fits for lattice parameter determination for (c) K_4C_{60} at 6 K and (d) Rb_4C_{60} at 4 K. The measured data on these latter two graphs are shown by blue dots, the fits by blue lines, and the difference plots by black lines.

ented along either the *a* or *b* axes (*static Jahn-Teller state*). This scenario is, however, not the only possible geometry whose spatial average results in a tetragonal crystal. Molecules distorted either along the C_3 or the C_5 axis can form an ordered array resulting in a fourfold axis in the *c* direction (*staggered static Jahn-Teller state*). The molecular principal axis of a D_{3d} or D_{5d} anion cannot be parallel with the crystallographic axes, but must be arranged such that the overall average gives an $I4/mmm$ structure. The transition from static to staggered static state occurs through pseudorotation and vibration, i.e., the coordinates of the individual carbon atoms change only slightly and there is no reorientation of the molecule as a whole. If there are several configurations with small energy barriers between them (compared to the energy of thermal motion), the balls can assume many of these configurations dynamically and thus the *dynamic Jahn-Teller state* is formed. The significance of pseudorotation increases as the amplitude of thermal motion becomes larger.

The detection of the distortion by diffraction methods demands extreme sensitivity, as the magnitudes in question are small. Paul *et al.*[26] found a quasi-axial elongation of 0.04 Å in $(PPN)_2C_{60}$, where the symmetry of the C_{60}^{2-} dianion is lowered to C_2. In the monovalent decamethylnickelocenium salt,[27] the symmetry was found close to D_{2h}, with a difference between maximum and minimum radii of 0.05 Å. These are static distortions in which the role of the bulky organic counterions and the inherent JT effect cannot be separated.[28] The largest distortion (defined as the difference between the smallest and the largest distance from the center of the ball) so far has been found in the ordered orthorhombic phase of Cs_4C_{60}; 0.076 Å at 300 K.[6] In K_4C_{60} Kuntscher *et al.*[8] put an upper limit of 0.04 Å on the difference between "equatorial" and "polar" radii. One must take into account, though, that in the case of a staggered static arrangement the directions of maximum and minimum radii are not necessarily the crystal axes, and in the dynamic case the difference is smeared out completely.

TABLE I. Lattice parameters of K_4C_{60} and Rb_4C_{60} at the lowest and highest measured temperatures.

	Rb_4C_{60}		K_4C_{60}	
T (K)	*a* (Å)	*c* (Å)	*a* (Å)	*c* (Å)
4–6	11.912(1)	11.007(1)	11.827(1)	10.746(1)
300	11.949(1)	11.011(1)	11.862(1)	10.757(1)

In Fig. 2 (bottom), we show the corresponding splitting of the molecular orbitals. In the icosahedral C_{60} molecule the lowest unoccupied molecular orbital (LUMO) [which becomes the highest occupied molecular orbital (HOMO) in the molecular ions] is a threefold degenerate t_{1u} orbital. We obtain a threefold splitting of this orbital in the cooperative static and static JT states and a twofold splitting in the staggered static and dynamic states. The lowest-energy final states for dipole transitions also derive from a threefold degenerate orbital, the even-parity t_{1g} one. Incidentally, the four

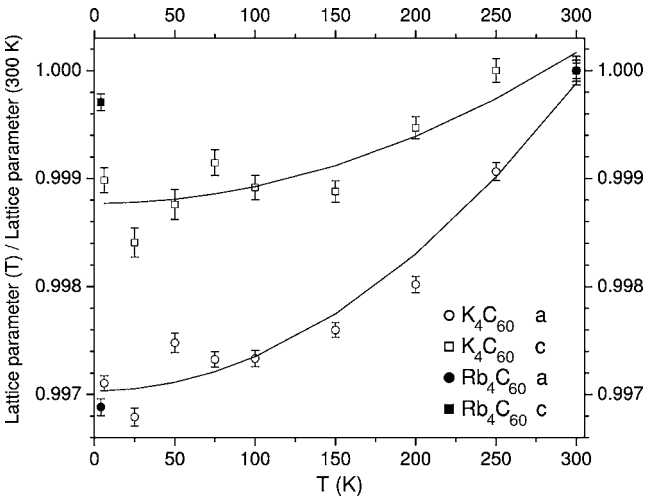

FIG. 4. Temperature-dependent lattice parameters normalized to the 300 K values of K_4C_{60} and Rb_4C_{60}. The lowest and highest temperature values are given in Table I. The solid lines are guides to the eye.

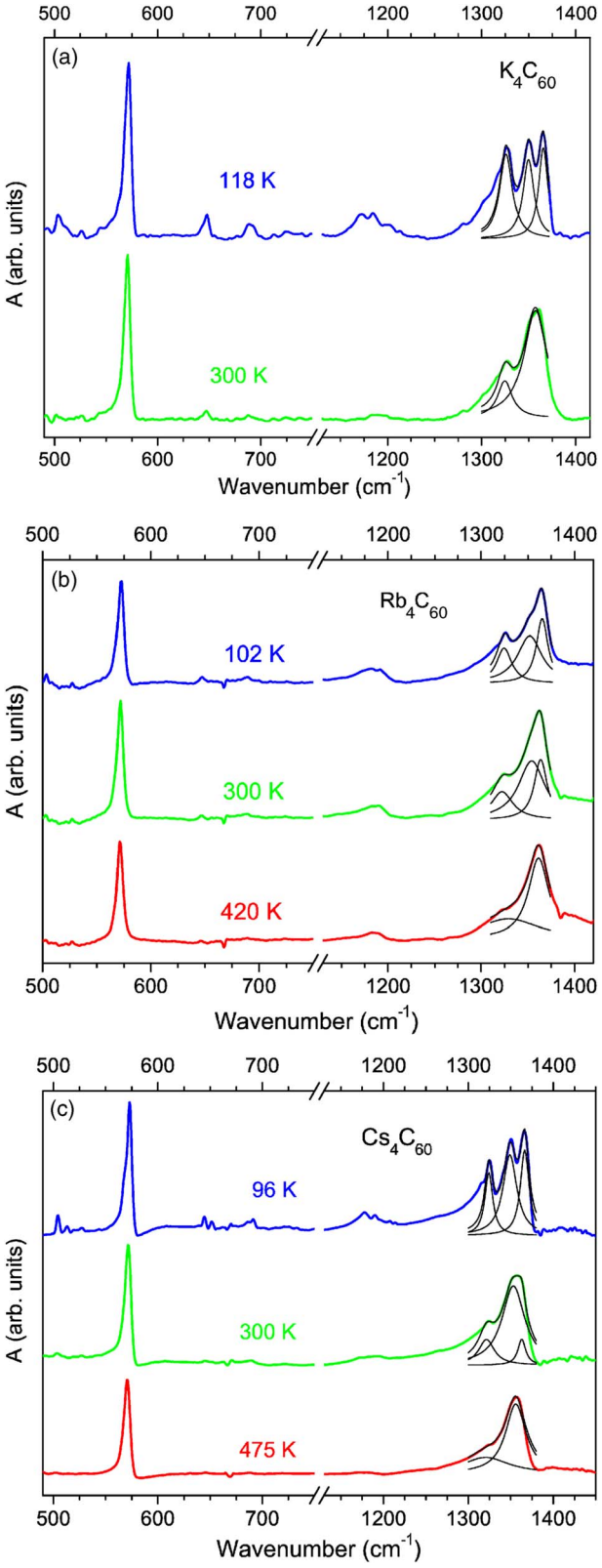

FIG. 5. (Color online) MIR spectrum of (a) K_4C_{60}, (b) Rb_4C_{60}, and (c) Cs_4C_{60} at selected temperatures above and below the change in symmetry (colored lines). The highest-frequency mode can be fitted with three Lorentzians at low temperature and two Lorentzians at high temperature (black lines). These splittings indicate a molecular symmetry change with temperature.

infrared-active vibrations of C_{60} also show T_{1u} symmetry, therefore the discussion can proceed along the same lines.

Further complications arise if we take into account that the fullerene balls are capable of rotation around several axes. The simplest scenario would be that occasional reorientational jumps between the two standard orientations (around the C_2 axis) would average out the symmetry from D_{2h} to D_{4h}. We know from inelastic neutron scattering in K_3C_{60},[29] however, that the rotation between standard orientations occurs with a much higher probability around a C_3 axis. Structural studies and modeling[8] in A_4C_{60} indicated that rotation around the C_2 axis is hindered because of unfavorable alkali atom-carbon distances. Thus we suggest that dynamic disorder in A_4C_{60} salts is the result of reorientation around the threefold axes.

III. EXPERIMENT

A_4C_{60} systems have been prepared previously either by solid-state synthesis[30–32] or by a liquid ammonia route.[7] We used a solid-state synthesis for all three alkali salts by reacting stoichiometric amounts of the alkali metal with C_{60} at 350 °C in a steel capsule. The reaction was followed using powder x-ray diffraction and MIR spectroscopy. The reaction mixture required heating for 10 to 14 days with one intermediate sample regrinding in the case of K_4C_{60} and Cs_4C_{60}, and 20 days with three regrindings for Rb_4C_{60}, to achieve complete conversion. No impurities were observed in the K_4C_{60} and Rb_4C_{60} samples, while x-ray diffraction found less than 5% Cs_6C_{60} in Cs_4C_{60}.

Since fullerides are air sensitive, the synthesis and sample preparation was conducted in a dry box. For the MIR and NIR measurements, KBr pellets were pressed and transmittance spectra measured with the sample inside a liquid nitrogen cooled flow-through cryostat under dynamic vacuum. Spectra were recorded with resolution of 1 or 2 cm^{-1} in the MIR range using a Bruker IFS 28 spectrometer and 4 cm^{-1} in the NIR using a Bruker IFS 66v/S spectrometer.

Neutron scattering measurements were performed at the NIST Center for Neutron Research. Large amounts of materials were prepared for these experiments(2.4 g of K_4C_{60} and 1.1 g of Rb_4C_{60}) to achieve good counting statistics. Temperature dependent neutron diffraction data were collected on the BT1 diffractometer using a wavelength of $\lambda = 1.5403$ Å and a Q-range of 0.2–8.1 Å with the Cu(311) monochromator set at a 90° take-off angle and using in-pile collimation of 15 min of arc. Lattice parameters were extracted using the LeBail method.[33–35]

Low energy molecular librations were studied using the BT4 triple-axis spectrometer. We collected constant momentum transfer (Q) scans at $Q=5.5$ $Å^{-1}$ with a fixed incident energy of 28 meV. The incident beam was produced using a Cu(220) monochromator and a graphite filter for removal of higher order contamination. The scattered beam was analyzed using a graphite(004) crystal. The measured resolution with 60′-40′-40′-40′ collimation was 0.97 meV full width at half maximum. Samples were loaded in indium-wire-sealed aluminum and vanadium cylindrical cans. Sample temperature was controlled between 4 and 300 K with a closed cycle

TABLE II. The parameters of the Lorentzians fitted to the $T_{1u}(4)$ mode (wave number: ν^*, full width at half maximum: w, and integrated intensity: I). The intensities were normalized to the sum of intensities at 300 K.

	K_4C_{60}		Rb_4C_{60}			Cs_4C_{60}		
	118 K	300 K	102 K	300 K	420 K	96 K	300 K	475 K
$\nu_1^*(\text{cm}^{-1})$	1326±1	1324±1	1324±1	1322±1	1330±7	1324±1	1321±1	1323±3
$w_1(\text{cm}^{-1})$	15±2	17±4	19±2	28±3	82±31	11±2	21±2	55±12
I_1	3±1	2±1	2±1	2±1	4.3±4.1	4±1	3±1	4±3
$\nu_2^*(\text{cm}^{-1})$	1350±1	1358±1	1352±1	1354±2	1361±1	1349±1	1354±1	1356±1
$w_2(\text{cm}^{-1})$	14±2	33±2	32±4	33±3	27±2	20±2	34±2	27±2
I_2	3±1	9±3	2±1	5±2	5±2	9±2	15±2	10±1
$\nu_3^*(\text{cm}^{-1})$	1365±1		1365±1	1363±1		1366±1	1363±1	
$w_3(\text{cm}^{-1})$	12±2		15±2	17±2		12±2	10±2	
I_3	3±1		2±1	3±1		6±1	1.2±0.7	

helium refrigerator. In the analysis of librational spectra, background runs were first subtracted, the intensities were corrected for changes in the scattered energy contribution to the spectrometer resolution, and then the spectra were symmetrized for the thermal Bose factor. The corrected data were subsequently fitted using a Gaussian resolution function at zero energy transfer and two identical Lorentzians symmetrically located about the elastic line, and convoluted with the instrumental resolution function. Details of similar librational studies on other fullerides can be found in Ref. 29.

IV. RESULTS

A. Structure

Room temperature x-ray diffraction showed the crystal symmetries to be $I4/mmm$ in K_4C_{60} and Rb_4C_{60}, and $Immm$ in Cs_4C_{60}, in agreement with published results.[7,8] Temperature-dependent structural studies were reported only for Cs_4C_{60},[6] revealing an orthorhombic-tetragonal transition between 300 and 623 K. Previously, based on vibrational spectra in K_4C_{60},[11] we suggested a similar transition in the

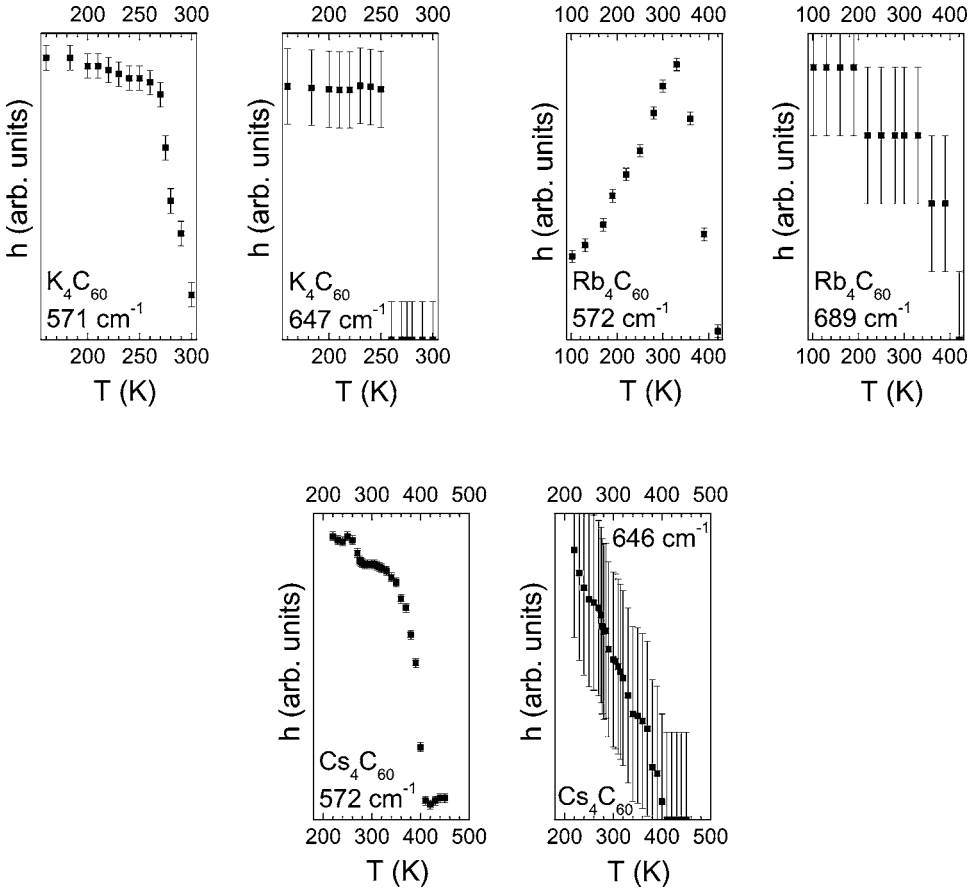

FIG. 6. Temperature dependence of the peak heights of selected MIR lines in K_4C_{60}, Rb_4C_{60}, and Cs_4C_{60}. Changes are apparent around 270, 330, and 400 K, respectively.

TABLE III. Peak positions (in cm^{-1}) of the Gaussians fitted to the NIR spectra. Note that the lowest frequency peak of Cs_4C_{60} at 151 and 298 K is a Lorentzian, which produced a better fit.

K_4C_{60}			Rb_4C_{60}				Cs_4C_{60}			
93 K	309 K	Ref. 3	89 K	300 K	480 K	Ref. 3	151 K	298 K	513 K	Ref. 3
7618±4	7464±3	7421	7275±7	7224±3	7006±6	7904	7730±3	7695±3	7071±6	7904
9499±10	9692±3	10082	9671±7	9682±3	9439±3	10324	9733±22	9719±24	9552±4	10324
10727±8							10680±50	10606±67		
12982±15		12582				12824	12571±19	12570±17		12824

two other alkali compounds. In order to draw a definitive conclusion on this hypothesis, we performed low-temperature neutron diffraction measurements on K_4C_{60} and Rb_4C_{60}. The resulting low- and high-temperature diffraction patterns are compared in Fig. 3. We found that the structure of both K_4C_{60} and Rb_4C_{60} remain tetragonal down to the lowest temperatures measured. The 4 and 300 K lattice parameter values from the LeBail analysis are given explicitly in Table I. The room-temperature data agree with those of Kuntscher *et al.*[8] for K_4C_{60} and Rb_4C_{60}.

We investigated the K_4C_{60} salt in detail, at several temperatures, to make sure we did not miss a possible tetragonal-tetragonal phase transition, similar to the one found in Rb_4C_{60} with increasing pressure.[36] The lattice parameters extracted at each temperature and normalized to the room-temperature values are shown in Fig. 4. As no significant change can be seen except for a small thermal contraction (an order of magnitude smaller than the pressure-induced change reported in Ref. 36), we can rule out even a tetragonal-tetragonal phase transition in K_4C_{60}.

B. Molecular vibrations

The MIR spectra of the three salts measured at room temperature and at characteristic temperatures unique for each salt are shown in Fig. 5. Since C_{60} is an icosahedral molecule, it has only four infrared active vibrations (at 528, 577, 1183, and 1429 cm^{-1}),[37] all of which belong to the T_{1u} representation. The shift and the splitting of the highest frequency $T_{1u}(4)$ mode has been used as the most sensitive indicator for charge transfer,[38] symmetry change,[39] and bonding[40] in fullerene compounds. The most prominent feature of our spectra is the splitting of this mode (shifted to 1350 cm^{-1} because of charge effects) indicating a lowering of symmetry from icosahedral. All spectra could be fitted with either two or three Lorentzians in this frequency range, and the results are summarized in Table II. The temperature dependence of the splitting of the $T_{1u}(3)$ mode around 1182 cm^{-1} was found to be the same as for the $T_{1u}(4)$ mode. In contrast, the two lower-frequency modes were not split at our resolution, instead, we observed a decrease in peak height and increase in linewidth of the $T_{1u}(2)$ mode at 571 cm^{-1} (Fig. 6). [We note that in pristine C_{60} below the orientational phase transition[41] no splitting was observed in the $T_{1u}(2)$ mode even at 0.4 cm^{-1} resolution and the splitting of the $T_{1u}(1)$ mode was less than 1 cm^{-1}. The latter mode is almost unobservable in the C_{60}^{4-} ion.[38]] The symmetry lowering from I_h also activates previously silent modes, appearing between 600 and 750 cm^{-1}. The intensity of these peaks increases on cooling. The temperature dependence of this increase can also be used to follow the symmetry change of the C_{60}^{4-} anion.

From Fig. 2, it follows that the T_{1u} modes split twofold in the D_{5d} and D_{3d} point groups, and threefold in the D_{2h} point group and since all split modes are infrared-active, this directly indicates the geometry. It is also clear that in all compounds, the distortion changes from the latter to the former upon warming. The temperature where this occurs depends on the counterion. From Fig. 6 the transition temperatures for K_4C_{60}, Rb_4C_{60}, and Cs_4C_{60} are approximately 270, 330, and 400 K, respectively, increasing with increasing cation size.

C. Electronic transitions

MIR spectra indicated a molecular symmetry change from D_{2h} to D_{3d}/D_{5d} on heating in all three compounds and electronic transitions should exhibit similar splitting. A splitting has been reported in NIR spectra of K_4C_{60} (Ref. 10) and was systematically investigated by transmission electron energy loss spectroscopy in a series of A_4C_{60} compounds.[2,3] The KBr pellet technique is not a particularly good method for quantitative evaluation in a broad frequency range, due to scattering effects in the pellets and inadequate determination of the optical path length. We nevertheless measured the NIR spectra of all the compounds at several temperatures and relate our findings to the EELS measurements by Knupfer and Fink.[3] Oscillator strengths in thin film transmission EELS studies can be compared more reliably between different materials; the frequency resolution of this method, on the other hand, is only 928 cm^{-1} compared to 4 cm^{-1} in the infrared spectra. Therefore we concentrate on the number and position of electronic excitations and will not attempt to draw any conclusion regarding line width or intensity.

Figure 7 shows overall (MIR/NIR) spectra of the three salts and C_{60}. It is apparent that there is a finite spectral weight even at low frequency, and its relative intensity decreases with increasing cation size. Knupfer and Fink[3] have identified this low-frequency excitation around 4000 cm^{-1} (0.5 eV), as a transition between Jahn-Teller split states (e.g, $e_u \rightarrow a_{2u}$ in Fig. 2) on *different* molecules. Intramolecular excitations between JT states are dipole forbidden, but in a Mott-Jahn-Teller picture, this energy, renormalized due to

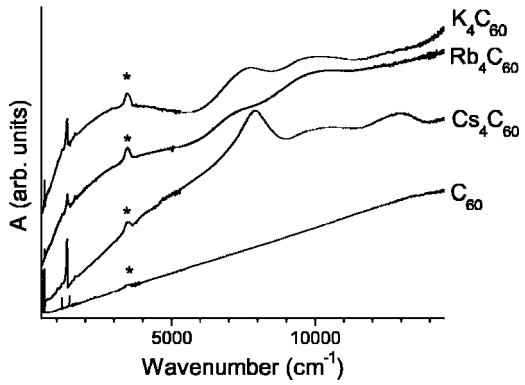

FIG. 7. Combined MIR-NIR spectra of K_4C_{60}, Rb_4C_{60}, Cs_4C_{60}, and C_{60} without background correction. The intermolecular transition at around 4000 cm^{-1} (broad background) gets weaker with increasing cation size. (The sharp peaks around 3700 cm^{-1}, denoted by asterisks, arise from atmospheric water absorption.)

intermolecular interactions, becomes the effective Hubbard repulsion term U_{eff}.[1] Such transitions have been observed in one-dimensional organic conductors.[42]

In order to better resolve the split NIR lines, we performed a baseline correction between 6000 and 14 000 cm^{-1} and fitted the remaining lines with Gaussians. The resulting fits are depicted in Fig. 8, and the parameters summarized in Table III. Four dipole allowed intramolecular transitions are expected in the case of D_{2h}, and two in the case of D_{3d}/D_{5d} (see Fig. 2). This is indeed seen in K_4C_{60} and in Cs_4C_{60} and corresponds to the MIR measurements at all temperatures. However, in Rb_4C_{60}, while the low-temperature spectra can be fitted with four Gaussians, the decomposition was not unambigous since these lines are broad and their splitting seems to be small. Comparing our parameters with those reported in Ref. 3 (Table III), we have the best agreement for Cs_4C_{60}, but instead of their three peaks we can identify four, as expected from symmetry. In the case of K_4C_{60} Ref. 3 found three similar lines as in Cs_4C_{60}, but we see two at low temperature and four at high temperature. We assume that the discrepancy originates in the baseline correction of the EELS data for the higher-lying electronic transition of C_{60}^{4-}. (Visual inspection of the spectra shown in Ref. 3 reveals that the 1.5 eV peak is much less pronounced in K_4C_{60} than in Cs_4C_{60} and Rb_4C_{60}.)

To summarize the above, vibrational and electronic spectra in all three salts indicate D_{2h} distorted C_{60}^{4-} ions at low temperature and D_{3d}/D_{5d} distorted ones at higher temperature at the time scale of the optical measurements. These methods cannot distinguish between individual configurations in the static or the staggered static Jahn-Teller state, nor can they detect transitions between them. These transitions occur via librational motion, which can be studied by inelastic neutron scattering.

D. Librations

Inelastic neutron scattering (INS) spectra were measured as a function of momentum transfer, Q, and energy transfer, E, at several temperatures for K_4C_{60} and Rb_4C_{60}. Figures 9(a) and 9(b) show spectra at 100, 200, and 300 K for K_4C_{60} and at 100 and 300 K for Rb_4C_{60} at a constant momentum transfer of $Q=5.5$ $Å^{-1}$. The solid symbols are the corrected experimental data and the lines are fits as described in the experimental details section. Well-defined peaks are observed at nonzero energy transfer at all temperatures in both fullerides and may be assigned to librational modes of C_{60}^{4-} ions based on the momentum transfer dependence of their intensities and peak widths. The Q-dependence of the inte-

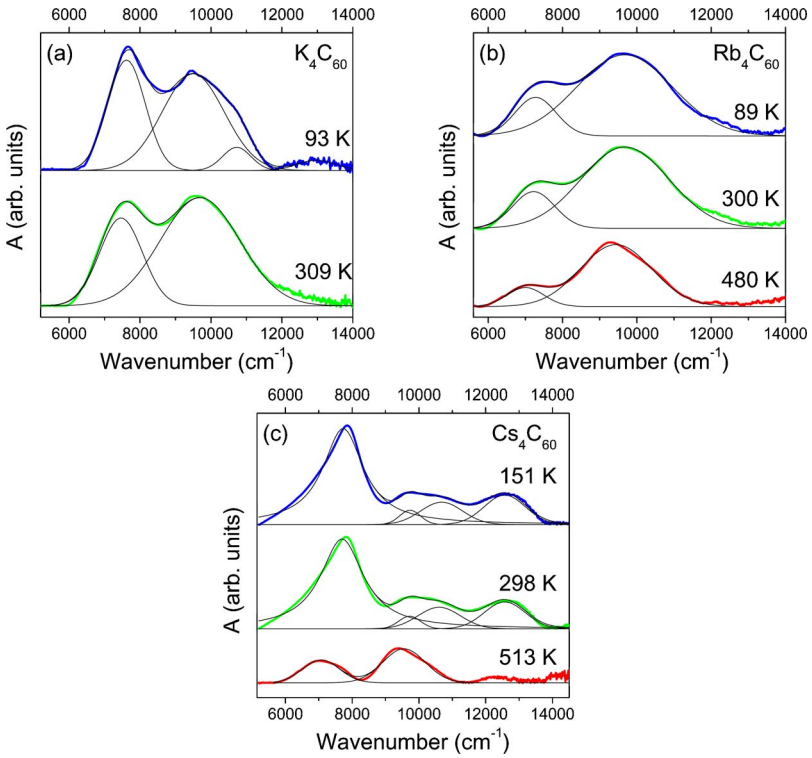

FIG. 8. (Color online) Baseline-corrected NIR spectrum of (a) K_4C_{60}, (b) Rb_4C_{60}, and (c) Cs_4C_{60} at selected temperatures (colored lines). The spectra were fitted with Gaussians, with the exception of the lowest frequency peak of Cs_4C_{60} at 151 and 298 K where a Lorentzian produced a better fit. These fits are shown with black lines.

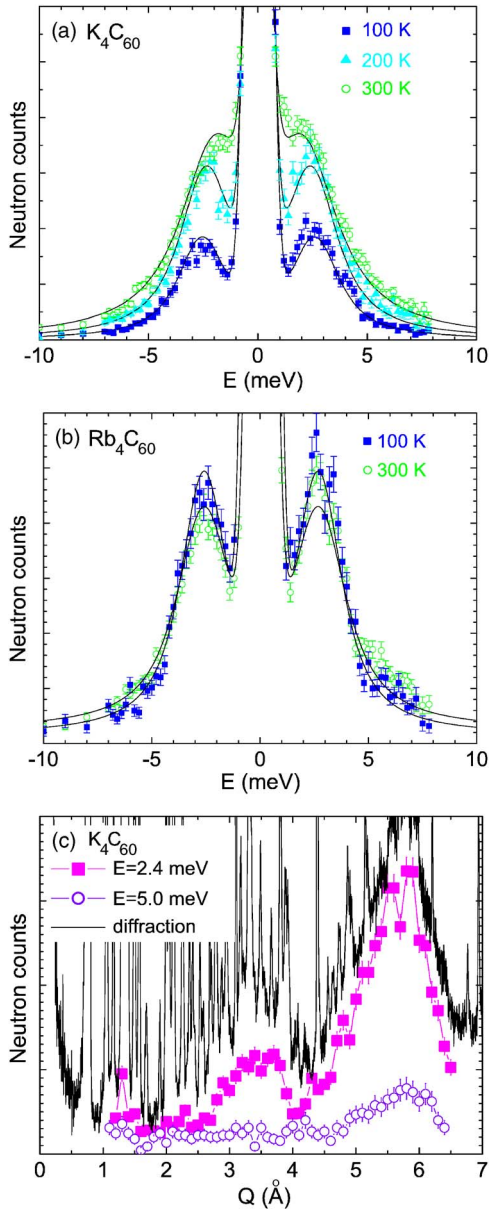

FIG. 9. (Color online) (a) Fixed momentum transfer scans of K_4C_{60} at 100, 200, and 300 K at $Q=5.5$ Å^{-1}. (b) Fixed momentum transfer scans of Rb_4C_{60} at 100 and 300 K at $Q=5.5$ Å^{-1}. Symbols are the measured data, lines are fits as described in the text. (c) Fixed energy transfer scans at $E=2.4$ and 5 meV of K_4C_{60} along with the neutron diffraction pattern scaled to emphasize the diffuse background.

grated intensity of the librational modes in fullerides is characteristic of the form factor of the C_{60} molecule and has been studied in detail in many fullerides; it provides unambiguous evidence for the assignment as librations.[43–45] Figure 9(c) shows Q-dependent data at fixed energy transfers of 2.4 and 5 meV for K_4C_{60}. The momentum transfer spectrum at $E=2.4$ meV is a reasonable substitute for the Q-dependent integrated intensity because the librational peak position and width are insensitive to Q according to our energy transfer spectra at a few other selected momentum transfers. The 2.4 meV peak displays the characteristic Q-dependence of

TABLE IV. Measured librational energies (E_{lib}) of K_4C_{60} and Rb_4C_{60}, calculated energy barriers of the reorientation (E_{barrier}), and root-mean-square librational amplitudes (Θ_{rms}) at 100 and 300 K.

	E_{lib} (meV)	E_{barrier} (meV)	Θ_{rms} (°)
K_4C_{60} 100 K	2.57±0.10	277±22	3.55±0.01
K_4C_{60} 300 K	2.00±0.10	168±17	7.85±0.02
Rb_4C_{60} 100 K	2.65±0.10	294±22	3.44±0.07
Rb_4C_{60} 300 K	2.64±0.10	293±22	5.96±0.01

the librational modes of fullerides with a small peak around $Q=3.5$ Å^{-1} and a larger peak around $Q=5.7$ Å^{-1}. These peaks are attributed to the nonzero Legendre polynomials with coefficients of $l=10$ and 18, respectively.[46] In contrast, the momentum transfer spectrum at 5 meV energy transfer does not show this behavior since it has much less librational character.

The main motivation for the low temperature diffraction experiments was to search for a possible structural phase transition similar to the order-disorder transition in Cs_4C_{60}.[6] Additional proof that there is no ordering of the C_{60}^{4-} between room temperature and 6 K in K_4C_{60} is presented by the large and temperature independent diffuse background. Figure 9(c) compares the diffuse background to the fixed energy transfer scans discussed above. As observed for other fullerides, the Q-dependence of the diffuse background of the diffraction is very similar to that of the librational peak, indicating disorder of the C_{60}^{4-} anions.[47]

The librational energies obtained by fitting the inelastic peaks can be found in Table IV. Following the arguments of Neumann *et al.*,[43] the rotational barrier between the two orientations can be estimated assuming that a simple sinusoidal hindrance potential can describe the rotational motion of the C_{60} anion. For small amplitudes of libration, the potential barrier is calculated as

$$E_{\text{barrier}} = \frac{E_{lib}^2}{B}\left(\frac{\Theta_{\text{jump}}}{2\pi}\right)^2,$$

where Θ_{jump} is the reorientation angle between neighboring potential minima, $B=0.364$ μeV is the rotational constant for C_{60}, and E_{lib} is the librational energy at a given Q and temperature. For Θ_{jump} we assume 44.5°, meaning that a rotation about the C_3 axis of the molecule—which is approximately in the [111] direction—brings the molecule from one standard orientation to the other. We obtain a value for the potential barrier $E_{\text{barrier}}=277$ meV for K_4C_{60} and 294 meV for Rb_4C_{60} based on the observed E_{lib} at 100 K. These estimated potential barriers are comparable to C_{60} and much smaller than in K_3C_{60} or Rb_6C_{60},[29] indicating smaller crystal fields in A_4C_{60}. The smaller crystal field is a consequence of the larger free volume in the A_4C_{60} compounds compared to A_3C_{60} or A_6C_{60}.[36]

The mean amplitude of the libration can also be calculated within the harmonic approximation from the librational energy via

$$\Theta_{rms} = \sqrt{\frac{4B}{E_{lib}} \coth\left(\frac{E_{lib}}{2kT}\right)}.$$

The obtained Θ_{rms} values are shown in Table IV. The $\Theta_{rms}=7.8°$ value of K_4C_{60} at room temperature is fairly large, which is readily seen when comparing it with the 7° value of C_{60} near its phase transition.[46] For C_{60}, 7° is considered the critical angle for orientational melting. There are additional similarities between the temperature dependence of the librational peak in K_4C_{60} and C_{60}. The librational mode of K_4C_{60} softens and widens with increasing temperature as in C_{60} (Ref. 46) and in the monomer phase of Na_2RbC_{60} below their phase transition temperature during which the rotation of the molecules becomes free.[46–48] In Rb_4C_{60} at room temperature, the librations increase only to 6° and the other trends are also absent.

Based on the above similarities in the temperature dependence of the librations between K_4C_{60} and C_{60} we raise the possibility that K_4C_{60} is close to an orientational melting transition at room temperature. This transition would be in accordance with the observed change of symmetry in the motion of C_{60}^{4-} found at 250 K by NMR in K_4C_{60}.[49] High temperature INS experiments are planned in order to search for this transition.

V. DISCUSSION

Two separate effects determine the distortion of fulleride anions in a lattice: the JT effect of the molecule and the crystal field of the external potential caused by the counterions. Our structural and spectroscopic results help to determine the relative importance of these two effects depending on cation size and temperature. We also discuss the importance of the two dynamic processes, pseudorotation and molecular reorientation, based on spectroscopy and neutron scattering.

The low-temperature phase of all three A_4C_{60} salts studied can be modeled by the constructive interaction of the JT effect and the external potential, resulting in D_{2h} distorted fulleride ions. The D_{2h} molecular point group is identical to the crystal space group $Immm$ (D_{2h}^{25}) of Cs_4C_{60} and the largest common subgroup of I_h and $I4/mmm$ (D_{4h}^{17}) of K_4C_{60} and Rb_4C_{60}. Accordingly, Cs_4C_{60} forms a true cooperative static Jahn-Teller state and the other two salts a static Jahn-Teller state with distorted ions randomly occupying the two standard orientations. Since the molecular symmetry is identical and the molecules are static at the time scale of the spectroscopic measurements, vibrational and electronic spectra are independent of the crystal structure. The reason why these structures are different has been given by Dahlke *et al.*[6] following Yildirim *et al.*:[24] to minimize repulsive interaction between cations and anions due to orbital overlap.[23] According to this model, the orientational order in the orthorhombic phase of Cs_4C_{60} appears to avoid close Cs-C contacts, which would arise in the disordered structure.[6] In the other two compounds where the free volume is larger, the two standard orientations remain but reorientation between them slows down. Dahlke *et al.*[6] estimated the critical value of the controlling parameter (closest cation-anion center distance minus the cation radius) to fall between the low-temperature phase of Cs_4C_{60} and Rb_4C_{60}. With increasing temperature, Cs_4C_{60} reaches this critical value and a phase transition to a tetragonal phase happens between 300 and 623 K.[6] The crystal structure of Cs_4C_{60} at high temperature and K_4C_{60} and Rb_4C_{60} at all temperatures are similar.[6,8] According to our infrared results, the *molecular* point group in each compound is changing from D_{2h} to D_{3d}/D_{5d} upon warming, the transition temperature increasing with cation size. Lacking structural data at intermediate temperatures, we cannot tell whether the symmetry change in Cs_4C_{60} coincides with the structural transition, but in K_4C_{60} and Rb_4C_{60} we definitely observe a change of molecular geometry *without* changing the crystal structure.

The D_{2h} distortion can only be realized when an external potential, like that of the surrounding cations, lowers its energy. As the temperature is raised, the lattice expands, and at the same time pseudorotation becomes more probable, both contributing to a competition between the molecular Jahn-Teller effect and the external potential. As the molecular ions decouple from the lattice, the tendency to behave as isolated ions gets stronger and thus the possibility of D_{3d}/D_{5d} distortions increases. The estimated distortion of C_{60}^{4-} ions is the largest among the fulleride ions, larger than in C_{60}^{3-},[6] which further explains the difference in electronic properties between the two types of compounds. The significance of this effect relative to the crystal field increases with increasing temperature and increasing cation-anion distance. The scaling of the transition temperatures with cation size corroborates this assumption.

In the following we consider four possible structural models, depicted schematically in Fig. 10. The dark background symbolizes the volume into which the molecule is confined by the crystal field; the growth of this area from model (1) to (4) indicates a decreasing strength of the crystal field due to heating or smaller cation size. The light blue areas represent the fulleride ions; the direction of the minor axis of an ellipse refers to the direction of the principal molecular axis. In the case of a D_{2h} distortion this principal axis intercepts two hexagon–hexagon bonds, while in the case of D_{3d} and D_{5d} distortions it goes through the centers of two hexagons and two pentagons, respectively [see Fig. 1(a)]. Thus the direction of the principal axis determines the point group of the molecule standing in a given orientation. This way the horizontal ellipse in the figure of model (3) corresponds to the pancake-shaped D_{2h} distortion. Ellipses in other directions should be considered as representing D_{3d} or D_{5d} distortions.

If the crystal field is very strong [model (1)], it causes a static D_{2h} distortion. It is possible, although not probable, that this distortion is identical to the pancake shape corresponding to the saddle point on the APES of isolated molecules. In a general case—like that of Cs_4C_{60}—the distorted molecule has a different shape. The clover shape of the light blue region in the figure represents that of the anion found in Cs_4C_{60} by neutron diffraction.[6] Model (1) works for both orthorhombic and tetragonal crystal fields since the molecular point group is the same in both cases. The tetragonal crystal structure requires the average of the atomic positions over the crystal to exhibit D_{4h} symmetry. As it has been mentioned earlier, one molecule cannot distort into this point

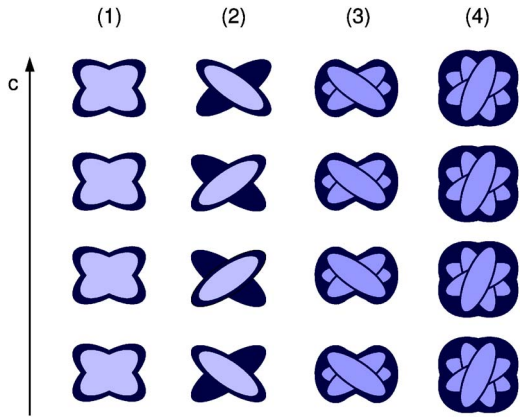

FIG. 10. (Color online) Possible structural models of Jahn-Teller distorted fulleride ions (light blue) in a crystal field. The dark background symbolizes the volume in which the molecule is confined by the crystal field. The figures within each column depict fulleride ions on different lattice points. The magnitude of the distortion of the fulleride ions is overemphasized for clarity. (1) Static D_{2h} distortion, following the shape of the crystal field. (2) Static D_{3d}/D_{5d} distortion. The direction of the distortions can be ordered (staggered static Jahn-Teller state) or disordered. (3) Dynamic distortion in preferred directions appearing in an anisotropic crystal field. Both pancake-shaped D_{2h} and D_{3d}/D_{5d} distortions are realized with time. (4) Free pseudorotation of the D_{3d}/D_{5d} distortion in a weak isotropic crystal field. The deeper blue of the molecules in models (3) and (4) represents a temporal average. This picture illustrates only the distortion of the anions; for their orientation see Fig. 2.

group, but the spatial average of D_{2h} molecules randomly distributed over two standard orientations will produce the required fourfold axis.

In models (2) and (3), the crystal field is weaker than in the previous case, thus it allows the appearance of the squeezed D_{3d}/D_{5d} distortions, which are the minima of the molecules' APES. The conversion between equivalent D_{3d}/D_{5d} distortions with the principal axis pointing in different directions could take place by pseudorotation through a pancake-shaped D_{2h} distortion.

In model (2), the intermediate D_{2h} distortion still leads to too short A-C distances, thus pseudorotation is not possible and the distortion is static. The distorted molecules can be arranged in the crystal either ordered in some way (staggered static state) or totally disordered regarding the direction of their principal axis.

In model (3) the crystal field is considerably weaker in some directions (e.g., in a and b) than in others, thus molecules can extend in these directions. This way distortions can appear not only in different directions but also with different point groups. The pancake-shaped D_{2h} distortion is present as the most favored distortion of the crystal field and the D_{3d}/D_{5d} distortions are present because they are preferred by the molecular JT effect. Although the molecule is not free to take up distortions in any direction, the allowed distortions can convert dynamically among themselves. The MIR spectrum of this state would contain five lines originating from each T_{1u} molecular mode: three corresponding to D_{2h} molecules and two to D_{3d}/D_{5d} molecules. Similarly, sixfold splitting should appear in the NIR spectrum. Since fitting spectra with many more parameters invariably yields a better fit, we cannot distinguish between states with only D_{2h} and with both D_{2h} and D_{3d}/D_{5d} distortions.

In model (4) the crystal field is very weak, thus the molecule can perform free pseudorotation in the crystal just like an isolated molecule. As the potential is very nearly isotropic, the pancake-shaped D_{2h} distortion is no longer favored, and only the D_{3d}/D_{5d} distortions appear.

Models (3) and (4) contain dynamical disorder of distorted molecules. IR spectroscopy only detects the individual distortions and not their average if the time scale of the spectroscopic excitations is smaller than the time scale of pseudorotation.

The low-temperature phase of the three A_4C_{60} salts corresponds to model (1), containing statically D_{2h} distorted molecules due to the strong crystal field. In Cs_4C_{60} the abrupt change of the crystal field at the phase transition can result in a simultaneous change of the molecular distortion, to any of the models (2), (3), or (4). Further heating will lead to states with gradually weakening crystal field, in the order: model (2) $\rightarrow$ model (3) $\rightarrow$ model (4). In K_4C_{60} and Rb_4C_{60} the absence of a phase transition indicates a continuous transition from model (1) to models with D_{3d}/D_{5d} molecules. Such a continuous transition cannot lead from model (1) to model (2), though. The explanation is as follows. The possible configurations of a molecule in a crystal are those of the isolated molecule (corresponding to the lowest energy points of the warped trough of the APES), and those preferred by the crystal field (D_{2h} distort ions with the shape preferred by the surroundings of the molecule). A continuous transition can lead from the former to the latter only if there is no high energy barrier between them. The intermediate configurations are the D_{2h} saddle points on the trough of the APES. As these configurations have high energy in model (2), no continuous transition can lead to this state. Because models (3) and (4) contain dynamically distorted molecules, we conclude that on heating a static-to-dynamic transition takes place in K_4C_{60} and Rb_4C_{60}.

Pseudorotation is not to be confused with molecular reorientation which we studied by inelastic neutron scattering. From the molecular point of view this motion is an abrupt rotation of the crystal field. During the rotation the distortion of the molecule should follow the change of the crystal field. Thus in the two standard orientations the direction of the distortions is different. INS data complement the spectroscopic results in two ways: they emphasize the possibility of the rotational motion around a C_3 axis, thus stressing its importance, and they prove the weakening of the crystal field with increasing temperature, through increasing librational amplitudes.

The results shown here are in good agreement with the ^{13}C-NMR spectra of Ref. 4. Above 150 K the reorientational motion observed in our NIS measurement could correspond to a rotation around one of the four C_3 axes of the molecule on the long time scale of NMR measurements. Thus when the axis of this rotation changes with a lower frequency than that of the NMR measurement, it causes the observed NMR line-shape characteristic of uniaxial motion.[4] Below 150 K the reorientational motion could be static on the NMR time scale leading to the observed line broadening. Around 250 K

the shape of the NMR line changes, which could correspond to the changing of the molecular symmetry from model (1) to model (3) or (4).

VI. CONCLUSIONS

MIR and NIR measurements showed that the same molecular geometry change is present in K_4C_{60}, Rb_4C_{60}, and Cs_4C_{60}: the point group of the C_{60}^{4-} molecular ion changes from D_{2h} to D_{5d} or D_{3d} on heating. Contrary to Cs_4C_{60}, where an orthorhombic-tetragonal transition takes place, we did not find a structural phase transition in K_4C_{60} and Rb_4C_{60}. The absence of a phase transition can be explained by the smaller cation-anion overlap which does not stabilize the orthorhombic structure.

Since the molecular geometry change in K_4C_{60} and Rb_4C_{60} is not coupled to a phase transition, the fundamental role of the molecular Jahn-Teller effect in the transition is obvious. On heating, the importance of the Jahn-Teller effect is increasing as the D_{2h} potential of the surrounding cations decreases and the number of accessible degrees of freedom increases. The weakening of the crystal field on heating is also indicated by the INS results.

Because of the dominance of the crystal potential in the D_{2h} distortion, this distortion is static. In the case of K_4C_{60} and Rb_4C_{60} we suggest that a dynamic Jahn-Teller state develops as the D_{3d}/D_{5d} distortions appear.

From the splitting of the electronic transition around 1 eV we conclude that the energy bands in the solid reflect the Jahn-Teller distortion of the molecular ions; the presence of the 0.5 eV feature, which is forbidden in the molecule and therefore must be assigned to intermolecular excitations, signals the importance of electron-electron correlations in the solid. We regard the simultaneous appearance of these two features as experimental proof of the Mott-Jahn-Teller insulator state.[1]

ACKNOWLEDGMENTS

We thank Gábor Oszlányi for his invaluable help with characterizing the samples by x-ray diffraction and most enlightening conversations. We also gratefully acknowledge useful discussions with Dan Neumann and Terrence Udovic. Financial support was provided by OTKA Grants No. T 034198 and No. T 049338 and NSF-INT Grant No. 9902050.

*Electronic address: klupp@szfki.hu
†Electronic address: kamaras@szfki.hu
‡Present address: Instituto de Ciencia de Materiales de Madrid (ICMM-CSIC), 28049 Cantoblanco, Madrid, Spain.

[1] M. Fabrizio and E. Tosatti, Phys. Rev. B **55**, 13465 (1997).
[2] M. Knupfer, J. Fink, and J. F. Armbruster, Z. Phys. B: Condens. Matter **101**, 57 (1996).
[3] M. Knupfer and J. Fink, Phys. Rev. Lett. **79**, 2714 (1997).
[4] V. Brouet, H. Alloul, S. Garaj, and L. Forró, Phys. Rev. B **66**, 155122 (2002).
[5] A. Wachowiak, R. Yamachika, K. H. Khoo, Y. Wang, M. Grobis, D.-H. Lee, S. G. Louie, and M. F. Crommie, Science **310**, 468 (2005).
[6] P. Dahlke and M. J. Rosseinsky, Chem. Mater. **14**, 1285 (2002).
[7] P. Dahlke, P. F. Henry, and M. J. Rosseinsky, J. Mater. Chem. **8**, 1571 (1998).
[8] C. A. Kuntscher, G. M. Bendele, and P. W. Stephens, Phys. Rev. B **55**, R3366 (1997).
[9] G. M. Bendele, C. A. Kuntscher, and P. W. Stephens, in *Molecular Nanostructures*, edited by H. Kuzmany, J. Fink, M. Mehring, and S. Roth (World Scientific, Singapore, 1998), p. 258.
[10] Y. Iwasa and T. Kaneyasu, Phys. Rev. B **51**, 3678 (1995).
[11] K. Kamarás, G. Klupp, D. B. Tanner, A. F. Hebard, N. M. Nemes, and J. E. Fischer, Phys. Rev. B **65**, 052103 (2002).
[12] C. C. Chancey and M. C. M. O'Brien, *The Jahn-Teller Effect in C_{60} and Other Icosahedral Complexes* (Princeton University Press, Princeton, 1997).
[13] H. A. Jahn and E. Teller, Proc. R. Soc. London, Ser. A **191**, 220 (1937).
[14] A. F. Hebard, M. J. Rosseinsky, R. C. Haddon, D. W. Murphy, S. H. Glarum, T. T. M. Palstra, A. P. Ramirez, and A. R. Kortan, Nature (London) **350**, 600 (1991).
[15] M. C. M. O'Brien, Phys. Rev. B **53**, 3775 (1996).
[16] J. L. Dunn and C. A. Bates, Phys. Rev. B **52**, 5996 (1995).
[17] S. Tomita, J. U. Andersen, E. Bonderup, P. Hvelplund, B. Liu, S. B. Nielsen, U. V. Pedersen, J. Rangama, K. Hansen, and O. Echt, Phys. Rev. Lett. **94**, 053002 (2005).
[18] A. B. Harris and R. Sachidanandam, Phys. Rev. B **46**, 4944 (1992).
[19] I. Lukyanchuk, N. Kirova, F. Rachdi, C. Goze, P. Molinie, and M. Mehring, Phys. Rev. B **51**, 3978 (1995).
[20] L. Forró and L. Mihály, Rep. Prog. Phys. **64**, 649 (2001).
[21] R. Kerkoud, P. Auban-Senzier, D. Jérome, S. Brazovskii, N. Kirova, I. Luk'yanchuk, F. Rachdi, and C. Goze, Synth. Met. **77**, 205 (1996).
[22] M. Ozaki and A. Takahashi, Chem. Phys. Lett. **127**, 242 (1986).
[23] J. E. Fischer and P. A. Heiney, J. Phys. Chem. Solids **54**, 1725 (1993).
[24] T. Yildirim, S. Hong, A. B. Harris, and E. J. Mele, Phys. Rev. B **48**, 12262 (1993).
[25] P. W. Stephens, L. Mihaly, P. L. Lee, R. L. Whetten, S.-M. Huang, R. Kaner, F. Diederich, and K. Holczer, Nature (London) **351**, 632 (1991).
[26] P. Paul, Z. Xie, R. Bau, P. D. W. Boyd, and C. A. Reed, J. Am. Chem. Soc. **116**, 4145 (1994).
[27] W. C. Wan, X. Liu, G. M. Sweeney, and W. E. Broderick, J. Am. Chem. Soc. **117**, 9580 (1995).
[28] C. A. Reed and R. D. Bolskar, Chem. Rev. (Washington, D.C.) **100**, 1075 (2000).
[29] D. A. Neumann, J. R. D. Copley, D. Reznik, W. A. Kamitakahara, J. J. Rush, R. L. Paul, and R. M. Lindstrom, J. Phys. Chem. Solids **54**, 1699 (1993).
[30] R. M. Fleming, M. J. Rosseinsky, A. P. Ramirez, D. W. Murphy, J. C. Tully, R. C. Haddon, T. Siegrist, R. Tycko, S. H. Glarum,

P. Marsh, G. Dabbagh, S. M. Zahurak, A. V. Makhija, and C. Hampton, Nature (London) **352**, 701 (1991).
[31] D. W. Murphy, M. J. Rosseinsky, R. M. Fleming, R. Tycko, A. P. Ramirez, R. C. Haddon, T. Siegrist, G. Dabbagh, J. C. Tully, and R. E. Walstedt, J. Phys. Chem. Solids **53**, 1321 (1992).
[32] D. M. Poirier, D. W. Owens, and J. H. Weaver, Phys. Rev. B **51**, 1830 (1995).
[33] A. Larson and R. V. Dreele, Los Alamos National Laboratory Report LAUR, 2000 (unpublished), pp. 86–748.
[34] B. H. Toby, J. Appl. Crystallogr. **34**, 210 (2001).
[35] H. D. A. Le Bail and J. L. Fourquet, Mater. Res. Bull. **23**, 447 (1988).
[36] A. A. Sabouri-Dodaran, M. Marangolo, C. Bellin, F. Mauri, G. Fiquet, G. Loupias, N. Mezouar, W. Crichton, C. Herold, R. Rachdi, and S. Rabii, Phys. Rev. B **70**, 174114 (2004).
[37] W. Krätschmer, K. Fostiropoulos, and D. R. Huffman, Chem. Phys. Lett. **170**, 167 (1990).
[38] T. Pichler, R. Winkler, and H. Kuzmany, Phys. Rev. B **49**, 15879 (1994).
[39] K. Kamarás, Y. Iwasa, and L. Forró, Phys. Rev. B **55**, 10999 (1997).
[40] A. M. Rao, P. C. Eklund, J.-L. Hodeau, L. Marques, and M. Nunez-Regueiro, Phys. Rev. B **55**, 4766 (1997).
[41] C. C. Homes, P. J. Horoyski, M. L. W. Thewalt, and B. P. Clayman, Phys. Rev. B **49**, 7052 (1994).
[42] J. B. Torrance, B. A. Scott, and F. B. Kaufman, Solid State Commun. **17**, 1369 (1975).
[43] D. A. Neumann, J. R. Copley, W. A. Kamitakahara, J. J. Rush, R. L. Cappelletti, N. Coustel, J. E. Fischer, J. P. McCauley, A. B. Smith III, K. M. Creegan, and D. M. Cox, J. Chem. Phys. **96**, 8631 (1992).
[44] C. Christides, K. Prassides, D. A. Neumann, J. R. Copley, J. Mizuki, K. Tanigaki, I. Hirosawa, and T. W. Ebbesen, Europhys. Lett. **24**, 755 (1993).
[45] D. Reznik, W. A. Kamitakahara, D. A. Neumann, J. R. D. Copley, J. E. Fischer, R. M. Strongin, M. A. Cichy, and A. B. Smith III, Phys. Rev. B **49**, 1005 (1994).
[46] J. R. D. Copley, D. A. Neumann, R. L. Cappelletti, and W. A. Kamitakahara, J. Phys. Chem. Solids **53**, 1353 (1992).
[47] C. Christides, D. A. Neumann, K. Prassides, J. R. D. Copley, J. J. Rush, M. J. Rosseinsky, D. W. Murphy, and R. C. Haddon, Phys. Rev. B **46**, 12088 (1992).
[48] K. Tanigaki, I. Hirosawa, T. Manako, J. S. Tsai, J. Mizuki, and T. W. Ebbesen, Phys. Rev. B **49**, 12307 (1994).
[49] G. Zimmer, M. Helmle, M. Mehring, and F. Rachdi, Europhys. Lett. **27**, 543 (1994).